Eur. J. Mineral., 37, 773–781, 2025 https://doi.org/10.5194/ejm-37-773-2025 © Author(s) 2025. This work is distributed under the Creative Commons Attribution 4.0 License.





Elasticity of CaSiO₃–CaTiO₃ perovskite at lower-mantle pressures

Ye Wu

School of Physics and Mechanics, Wuhan University of Technology, Wuhan 430070, China

Correspondence: Ye Wu (yew@whut.edu.cn)

Received: 16 March 2025 - Revised: 19 July 2025 - Accepted: 11 August 2025 - Published: 21 October 2025

Abstract. Calcium silicate perovskite (named davemaoite, Ca-Pv for short) is believed to be the third most abundant mineral in Earth's lower mantle. Knowledge of its elasticity is important to constrain velocities of pyrolite and basalt models in lower-mantle conditions and then decipher the origins of seismic signatures via comparison with observed seismic velocities. Here elasticities and sound velocities of cubic CaSiO₃–CaTiO₃ perovskites at lower-mantle pressures have been investigated by first-principles calculations. The incorporation of titanium into cubic Ca-Pv increases C_{11} but decreases C_{12} and C_{44} at high pressures. As a result, elastic moduli (K_S and G) and wave velocities (V_P and V_S) decrease with increasing Ti content. Cubic CaSiO₃ exhibits high-seismic-velocity anisotropies at low pressures, which gradually decrease with increasing pressure, reaching minimum values near the lowermost mantle. In contrast, Ti-bearing Ca-Pv shows an initial decrease in velocity anisotropies, followed by a progressive increase at higher pressures. Compositional effects on elastic properties and velocity anisotropies of cubic CaSiO₃–CaTiO₃ perovskites are significant at lower-mantle pressures. Considering the amounts of Ca-Pv in pyrolite and basalt models, Ti-bearing Ca-Pv may be responsible for the observed seismic velocity anomalies associated with subducted oceanic crust and a potential source of seismic anisotropies in the lower mantle.

1 Introduction

Knowledge of structures and physical properties of constituent minerals in the lower mantle is essential to model the density and sound velocities of pyrolite and subducted oceanic crust models. Comparisons between predicted seismic velocities and geophysical observations are crucial to discussions of the causes of seismic anomalies and dynamic processes in the lower mantle. However, a major source of uncertainty in the predicted seismic velocities of pyrolite has been the influence of davemaoite, also called cubic CaSiO₃ perovskite (Ca-Pv hereafter), on velocity (Murakami et al., 2012; Tschauner et al., 2021). Cubic Ca-Pv is believed to be the third most abundant mineral, as it comprises 5 vol. %-10 vol. % and 24 vol. %-29 vol. % of pyrolite and basalt models in the lower mantle, respectively (Ricolleau et al., 2010; Irifune et al., 2010). However, there are few reliable measurements of its sound velocities in lower-mantle conditions because it is technically challenging to carry out static compression experiments in lower-mantle conditions.

As shown in Fig. S1 in the Supplement, CaSiO₃ is stable in the wollastonite structure in ambient conditions and transforms into breyite at pressures above ~ 4 GPa (Essene, 1974). Breyite decomposes into larnite (Ca₂SiO₄) and titanite (CaSi₂O₅) at pressures exceeding ~ 8 GPa (Gasparik et al., 1994). These two phases subsequently react to form the perovskite phase above \sim 13 GPa (Sueda et al., 2006), where tetragonal Ca-Pv is stable below ~ 500 K, and the cubic Ca-Pv becomes stable above this temperature (Komabayashi et al., 2007; Sagatova et al., 2021; Yin et al., 2023). Experimental studies at high pressure and room temperature on the elasticity of tetragonal Ca-Pv (space group: I4/mcm) propose that it might explain the seismic anomalies observed in the deep mantle (Li et al., 2004; Kudo et al., 2012). However, both experimental and theoretical studies on the phase stability of CaSiO₃ show that CaSiO₃ adopts a cubic perovskite structure (space group: $Pm\bar{3}m$) in lower-mantle conditions (Komabayashi et al., 2007; Stixrude et al., 2007). Since cubic Ca-Pv is unquenchable in ambient conditions, in situ experimental studies at high pressure and high temperature on its elasticity are technically challenging. As recently as 2019, Gréaux et al. (2019) reported in situ X-ray diffraction and sound velocity measurements on cubic Ca-Pv of up to 23 GPa and 1700 K. They found that cubic Ca-Pv has a smaller shear modulus than the tetragonal phase, which leads to substantially lower sound velocities of subducted basalt. This further supports the hypothesis of accumulation of basaltic crust in the uppermost lower mantle, which is associated with the observed low-seismic-velocity signatures. Soon after, Thomson et al. (2019) reported sound velocities of (Ti-bearing) Ca-Pv at ~ 12 GPa and up to 1500 K. By combining the new results with literature data and extrapolating, they proposed that seismic velocities of Ca-Pv can explain large low-shearvelocity provinces observed in the lower mantle (Garnero et al., 2016).

Since it is difficult to experimentally investigate the elastic properties of Ca-Pv in lower-mantle conditions, it is essential to employ computational methods. Karki and Crain (1998) reported elastic properties of cubic Ca-Pv by firstprinciples calculations in static (0 K) conditions. Stixrude et al. (2007) investigated elasticities of cubic and tetragonal Ca-Pv using static calculations and mean field theory. They proposed that tetragonal Ca-Pv has a much smaller shear modulus than cubic Ca-Pv. Additionally, Li et al. (2006) reported the elasticity of tetragonal Ca-Pv in lower-mantle conditions by means of first-principles molecular dynamics simulations. Later, the elasticity of cubic Ca-Pv in lower-mantle conditions was also studied using first-principles molecular dynamics. Kawai and Tsuchiya (2015) demonstrated that cubic Ca-Pv had a smaller shear modulus and slower sound velocities than bridgmanite. This suggests that Ca-Pv-rich material can produce low-seismic-velocity anomalies in the lower mantle. Both theoretical results and experimental extrapolations show that Ca-Pv with a small shear modulus may contribute to low seismic velocity in subducted basalt.

Ca-Pv in mid-ocean ridge basalt (MORB) contains up to 28 wt % TiO₂ in lower-mantle conditions (Litasov and Ohtani, 2005; Hirose and Fei, 2002; Ricolleau et al., 2010; Ono et al., 2001). In contrast, Ca-Pv in pyrolite contains a maximum of 3 wt % TiO₂ in the lower mantle (Hirose, 2002; Kesson et al., 1998). Additionally, up to 2.9 wt % TiO₂ has been reported in Ca-Pv inclusions found in deep diamond (Nestola et al., 2018; Walter et al., 2011). Notably, the incorporation of Ti stabilizes the tetragonal phase of CaSi_{0.6}Ti_{0.4}O₃ up to 1200 K at 12 GPa (Thomson et al., 2019). This indicates that tetragonal-cubic phase transition in Ti-bearing Ca-Pv occurs in higher-P-T conditions than it does in pure CaSiO₃ and may be associated with elastic anomalies of Ca-Pv. The incorporation of Ti in Ca-Pv may have a significant effect on its elastic properties. However, there are limited experimental studies on the elasticity of Tibearing Ca-Pv, and direct measurements of sound velocity under lower-mantle conditions remain challenging. Therefore, theoretical investigations into the elastic properties of CaSiO₃–CaTiO₃ perovskites are both essential and significant for advancing our understanding of the mineralogy and dynamics of Earth's lower mantle.

2 Computational methods

First-principles calculations based on density functional theory (DFT) were performed using the Vienna ab initio simulation package (VASP) in static conditions (Kresse and Furthmüller, 1996; Kresse and Joubert, 1999). The interaction between ions and electrons was described by the projector augmented-wave (PAW) method (Blöchl, 1994). The Ceperley–Alder exchange correlation potential of the local density approximation (LDA) parametrized by Perdew and Zunger was selected in this study (Ceperley and Alder, 1980; Perdew and Zunger, 1981), since it yields better agreement with the experimental equation of state (Stixrude et al., 2007). The kinetic energy cut-off was set to 1000 eV, and the energy convergence criterion was 10^{-6} eV. The Monkhorst–Pack scheme was used for Brillouin zone sampling (Monkhorst and Pack, 1976).

According to phase diagram of the CaSiO₃-CaTiO₃ system (Kubo et al., 1997), cubic Ca-Pv $(Pm\bar{3}m)$ is considered in this study. A $2 \times 2 \times 2$ supercell (40 atoms) of the conventional cubic unit cell is built (Tschauner et al., 2021). Four structural configurations, 8CaSiO₃-0CaTiO₃ (CaSiO₃), 7CaSiO₃-1CaTiO₃ (CaSi_{0.875}Ti_{0.125}O₃), 6CaSiO₃–2CaTiO₃ (CaSi_{0.75}Ti_{0.25}O₃), and 4CaSiO₃-4CaTiO₃ (CaSi_{0.5}Ti_{0.5}O₃), were considered (Fig. 1). For all structural configurations, Si atoms are substituted by Ti atoms in the most dispersed way possible to lower total energy. The k-points grid was set to $4 \times 4 \times 4$ for cubic Ca-Pv. Structural relaxations were performed at various unit-cell volumes, where unit-cell parameters and atomic positions were allowed to relax to obtain the minimum total energy. The obtained minimum total energies (E) at different volumes (V) were fitted to the third-order finite strain equation to obtain unit-cell volume (V_0) , isothermal bulk modulus (K_{T0}) , its pressure derivative (K'_{T0}) , and energy (E_0) at zero pressure (Birch, 1978; Davies, 1974). Once the equilibrium structure at a given volume was obtained, the structure was strained by applying compressional and shear strains of ± 0.01 , then the stress tensor in the strained structure was calculated. The elastic constants were determined by the ratios of deviatoric stress to applied strain.

It is noteworthy that the method of determining elastic constants described above assumes that the Ca-Pv has a $Pm\bar{3}m$ symmetry. Strictly, this assumption is incorrect as some of Si atoms have been replaced by Ti atoms. The magnitude of the effect of the broken symmetry on elastic constants has been assessed by examination of the stress tensor matrices. The deviations from the expected cubic symmetry are sufficiently small (Table S1 in the Supplement).

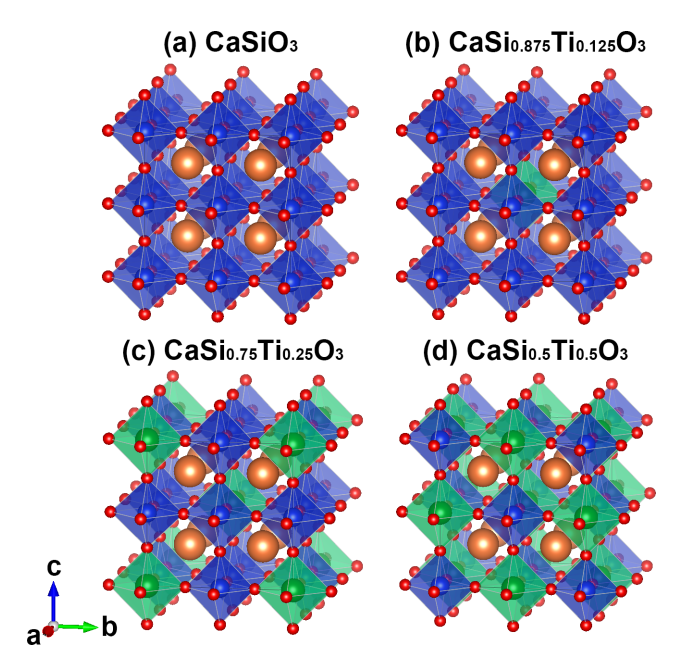


Figure 1. Four structural configurations of cubic CaSiO₃–CaTiO₃ perovskites with compositions of CaSiO₃, CaSi_{0.875}Ti_{0.125}O₃, CaSi_{0.75}Ti_{0.25}O₃, and CaSi_{0.5}Ti_{0.5}O₃.

3 Results and discussion

Three independent elastic constants, C_{11} , C_{12} , and C_{44} for the cubic Ca-Pv, are determined up to 130 GPa. The calculated elastic constants are analyzed using finite strain theory as follows (Birch, 1978; Davies, 1974):

$$C_{ij} = (1+2f)^{\frac{7}{2}} \left[C_{ij0} + a_1 f + \frac{1}{2} a_2 f^2 \right] + a_3 P, \tag{1}$$

$$a_1 = 3K_0 \left(C'_{ij} - a_3 \right) - 7C_{ij0}, \tag{2}$$

$$a_2 = 9K_0^2C_{ij}'' + 9K_0'K_0\left(C_{ij}' - a_3\right)$$

$$-48K_0\left(C'_{ij}-a_3\right)+63C_{ij0},\tag{3}$$

$$f = \frac{1}{2} \left[\left(\frac{V_0}{V} \right)^{\frac{2}{3}} - 1 \right],\tag{4}$$

where subscript 0 denotes values at zero pressure and prime denotes pressure derivatives; f is the finite strain; a_3 equals 3 for C_{11} and 1 for C_{12} and C_{44} ; and the parameters K_0 , K_0 ', and V_0 are taken from the E-V fitting of third-order finite strain equation. A third-order equation is used for C_{11} and C_{12} assuming $C_{ij}'' = 0$, while a fourth-order equation is used for C_{44} . The adiabatic bulk (K) and shear (G) moduli of cubic Ca-Pv are calculated by means of Voigt–Reuss–Hill

approximation (Hill, 1952):

$$K = \frac{K_{\rm V} + K_{\rm R}}{2},\tag{5}$$

$$G = \frac{G_{\rm V} + G_{\rm R}}{2},\tag{6}$$

$$K_{\rm V} = K_{\rm R} = \frac{C_{11} + 2C_{12}}{3},\tag{7}$$

$$G_{\rm V} = \frac{(C_{11} - C_{12}) + 3C_{44}}{5},\tag{8}$$

$$G_{\rm R} = \frac{5C_{44}(C_{11} - C_{12})}{4C_{44} + 3(C_{11} + C_{12})},\tag{9}$$

where subscripts "V" and "R" denote Voigt and Reuss, respectively. The obtained shear modulus is analyzed using the fourth-order finite strain equation:

$$G = (1+2f)^{\frac{5}{2}} \left[G_0 + b_1 f + \frac{1}{2} b_2 f^2 \right], \tag{10}$$

$$b_1 = 3K_0G_0' - 5G_0, (11)$$

$$b_2 = 9 \left\{ K_0^2 \left[G_0'' + \frac{1}{K_0} \left(K_0' - 4 \right) G_0' \right] + \frac{35}{9} G_0 \right\}. \tag{12}$$

Since calculations are performed in static conditions (0 K), the adiabatic bulk modulus (K_S) is equal to the isothermal bulk modulus (K_T) . Thus, parameter K without a subscript is used in these equations. The calculated K_{S0} via Voigt–Reuss–Hill approximation is very close to K_{T0} (Table 2). The isotropic aggregate compressional (V_P) and shear (V_S) wave velocities of Ca-Pv are then evaluated from the bulk and shear moduli and the density ρ as follows:

$$V_{\rm P} = \sqrt{\frac{K + \frac{4}{3}G}{\rho}},\tag{13}$$

$$V_{\rm S} = \sqrt{\frac{G}{\rho}}.$$
 (14)

All elastic constants increase with increasing pressure, and no elastic instability is found up to 130 GPa (Fig. 2). For different compositions, the individual elastic constants follow similar trends with pressure. The elastic constants at zero pressure and their pressure derivatives are listed in Table 1. The C'_{11} increases but C'_{12} and C'_{44} decrease with an increasing molar fraction of CaTiO₃. This indicates that increasing Ti content in cubic Ca-Pv has an opposite effect on C_{11} and C_{12} (C_{44}). As a result, the elastic moduli ($K_{\rm S}$ and G) and wave velocities ($V_{\rm P}$ and $V_{\rm S}$) increase at high pressures (Figs. 2b and 3b). The elastic moduli and wave velocities of cubic Ca-Pv with different compositions have similar trends with pressure. In general, the addition of Ti in cubic Ca-Pv makes elastic moduli (except for C_{11}) and wave velocities smaller with respect to pure cubic CaSiO₃.

The calculated density, unit-cell volume, and elastic moduli and their pressure derivatives, together with previous lit-

Composition	C ₁₁ (GPa)	C'_{11}	C ₁₂ (GPa)	C'_{12}	C ₄₄ (GPa)	C'_{44}	C'' ₄₄
CaSiO ₃	411.4	7.24	167.8	2.58	221.5	1.77	-0.016
CaSi _{0.875} Ti _{0.125} O ₃	410.8	7.38	157.2	2.52	195.3	1.59	-0.017
CaSi _{0.75} Ti _{0.25} O ₃	413.2	7.49	149.2	2.47	176.4	1.38	-0.016
CaSi _{0.5} Ti _{0.5} O ₃	406	7.65	137.3	2.4	142.1	1.14	-0.014

Table 1. The elastic moduli and their pressure derivatives of cubic Ca-Pv at zero pressure.

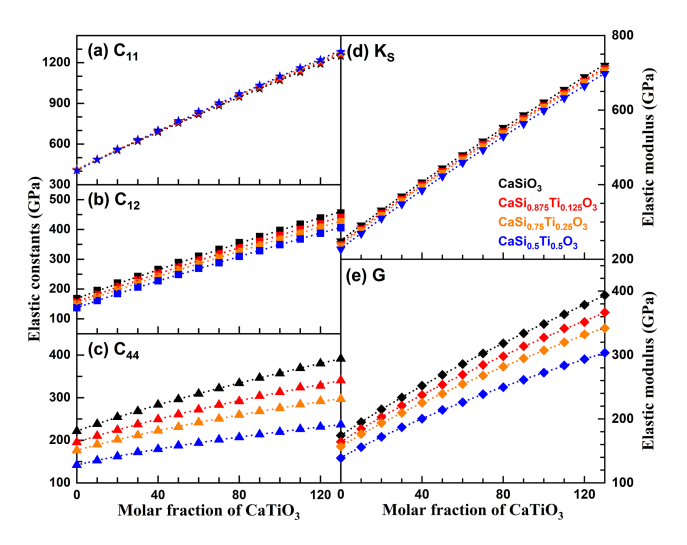


Figure 2. Elastic moduli of cubic CaSiO₃–CaTiO₃ perovskites at high pressures. Black, red, orange, and blue symbols represent CaSiO₃, CaSi_{0.875}Ti_{0.125}O₃, CaSi_{0.75}Ti_{0.25}O₃, and CaSi_{0.5}Ti_{0.5}O₃, respectively. The dotted curves are the results of fitting finite strain equations to the data (Birch, 1978; Davies, 1974).

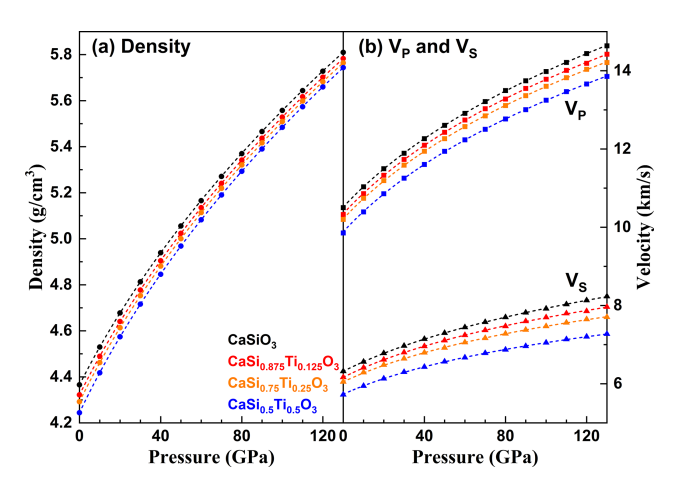


Figure 3. Densities (**a**) and wave velocities (**b**) of cubic CaSiO₃–CaTiO₃ perovskites at high pressures. Black, red, orange, and blue symbols represent CaSiO₃, CaSi_{0.875}Ti_{0.125}O₃, CaSi_{0.75}Ti_{0.25}O₃, and CaSi_{0.5}Ti_{0.5}O₃, respectively. The dashed curves are the best fit of the Eulerian finite strain equation (Birch, 1978; Davies, 1974).

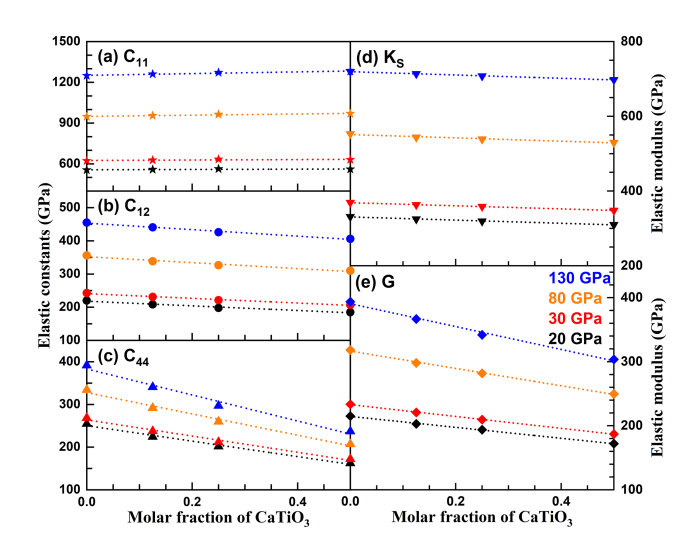


Figure 4. Elastic moduli of cubic CaSiO₃–CaTiO₃ perovskites at 20 GPa (black), 30 GPa (red), 80 GPa (orange), and 130 GPa (blue). Symbols and dotted lines are calculated values and linear fitting results, respectively.

erature values of Ca-Pv, are summarized in Table 2. The volume per formula of Ca-Pv increases with an increasing molar fraction of CaTiO₃. However, it is important to mention that these Ca-Pv phases have different crystal structures. The Ks_0 and K'_S of cubic CaSiO₃ obtained in this study are comparable to those of theoretical calculations and experimental measurements considering the trade-off between K_{T0} and K'_{T} (Karki and Crain, 1998; Kawai and Tsuchiya, 2015; Stixrude et al., 2007; Li et al., 2006; Gréaux et al., 2019). The values of G_0 and G' of cubic CaSiO₃ derived in this study are in good agreement with those of other computational studies but larger than those reported by Gréaux et al. (2019) based on experiments because of the systematic overestimations of elastic moduli by LDA calculations. The values of K_{S0} and G_0 of cubic CaSi_{0.5}Ti_{0.5}O₃ obtained with our computations are also larger than those of experimental studies due to the same reason as mentioned before (Sinelnikov et al., 1998). In general, both K_{S0} (K_{T0}) and G_0 of Ca-Pv decrease with an increasing molar fraction of CaTiO₃ demonstrated by both experimental measurements and first-principles calculations.

The density as a function of the molar fraction of CaTiO₃ has been fitted with a second-order polynomial, whereas the elastic moduli and wave velocities exhibit linear rela-

Table 2. Density, volume per formula, and elastic moduli at zero pressure and their pressure derivatives of Ca-Pv from this study and the previous literature.

Reference	Phase	Composition	d		K_{T0}	$K_{ op}^{\prime}$	K_{S0}	K_{ς}'	\mathcal{S}_0	Ć	, B	$P_{\text{max}}/T_{\text{max}}$	Method
			$(g cm^{-3})$	(\mathring{A}^3)		•		מ					
Theoretical calculations													
This study ^a	Cub	CaSiO ₃ CaSi _{0.875} Ti _{0.125} O ₃ CaSi _{0.75} Ti _{0.25} O ₃ CaSi _{0.5} Ti _{0.5} O ₃	4.3654 4.3216 4.2917 4.2441	44.19 45.58 46.86 49.33	249.0 241.7 237.2 226.8	4.14 4.16 4.16 4.15	250.8 242.5 237.7 228.5	1 1 1 1	174.2 164.2 157 139.5	2.16 2.07 1.94 1.75	-0.0149 -0.0164 -0.0163 -0.0158	130 GPa/0 K	DFT/LDA
Kawai and Tsuchiya (2015) Stixrude et al. (2007) Karki and Crain (1998) Li et al. (2006)	Cub Cub Cub Tet	CaSiO ₃	4.2648 4.3840 4.2544 4.2339	45.23 44 45.34 45.56	1 1 1 1	1 1 1 1	224 252 241 236.6	4.4 4.1 4.14 3.99	157 171 164 135	1.65 2.1 - 1.65	1 1 1 1	180 GPa/4000 K 220 GPa/0 K 140 GPa/0 K 123 GPa/4000 K	DFT+MD/LDA DFT/LDA DFT/LDA DFT+MD/GGA
Experiments													
Chao et al. (2024)	Tet	CaSi _{0.83} Ti _{0.17} O ₃ CaSi _{0.75} Ti _{0.25} O ₃	4.157(9)	47.7(1)	224(2) 205(4)	4 ^d	1 1	1 1	1 1	1 1	1 1	82 GPa/300 K 64 GPa/300 K	DAC+XRD
Sinelnikov et al. (1998)	Cub	CaSi _{0.49} Ti _{0.51} O ₃ CaSi _{0.23} Ti _{0.77} O ₃	4.139(2) 4.045(1)	50.65(2) 53.94(2)	185(5)	4 ^d	185(2) 182(3)	1 1	109(1)	1 1	1 1	8 GPa/300 K Ambient	LVP + XRD + UI
Sun et al. (2022)			4.23(2)	45.6(2)	229(4)	4 ^d	ı	ı	ı	ı	ı	199 GPa/300 K	DAC+XRD
Thomson et al. (2019) ^b			4.184(5)	46.10(6)	224(4)	4 _q	I	I	107(6)	1.44(8)	I	12 GPa/300 K	LVP + XRD + UI
Gréaux et al. (2019)			4.232(4)	45.58(4)	I	I	228(5)	3.7(4)	116(3)	1.3(2)	I	23 GPa/300 K	LVP + XRD + UI
Chen et al. (2018)	Ę	CaSiO	4.166(9)	46.3(1)	223(6)	4 _d	1	1	I	I	I	62 GPa/300 K	DAC + XRD
Kudo et al. (2012)	š	Carono 3	I	I	I	I	I	I	116(2)	1.20(2)	I	133 GPa/300 K	DAC + BS
Ono et al. (2004) ^c			4.20(4)	45.9(4)	235(9)	4 _d	ı	ı	I	I	I	96 GPa/300 K	DAC + XRD
Shim et al. (2002)			4.232(4)	45.58(4)	255(5)	4 ^d	1	I	I	I	I	46 GPa/300 K	DAC + XRD
Mao et al. (1989)			4.252(8)	45.37(8)	281(4)	4 _d	I	I	I	1	I	134 GPa/300 K	DAC + XRD
Gréaux et al. (2019)			4.232(4)	45.58(4)	ı	ı	248(3)	4.2(2)	126(1)	1.6(1)	ı	23 GPa/1700 K	LVP + XRD + UI
Sun et al. (2016)			4.249(9)	45.4(1)	249(4)	4 _d	I	1	I	I	I	151 GPa/2600 K	DAC + XRD
Noguchi et al. (2013)	Cub	CaSiO ₃	4.15(3)	46.1(3)	208(8)	4 _d	I	I	I	I	I	127 GPa/2300 K	DAC + XRD
Shim et al. (2000)			4.232(4)	45.58(4)	236(4)	3.9(2)	I	1	I	I	I	96 GPa/2419 K	DAC + XRD
Wang et al. (1996)			4.232(4)	45.58(4)	232(8)	4.8(3)	I	I	I	I	I	$13\mathrm{GPa/1600K}$	LVP + XRD
Truffet et al. (2023)			4.046(7)	55.8(1)	180.6(4)	4 ^d	ı	ı	I	I	I	60 GPa/2600 K	DAC + XRD
Guennou et al. (2010)	Orth	CaTiO ₃	4.046(7)	55.8(1)	181.0(6)	4 _d	1	1	I	I	I	60 GPa/300 K	DAC + XRD
Sinelnikov et al. (1998)			4 047(2)	55 78(3)	170(5)		173(2)	ı	106(1)	ı	1	9 CD2/300 V	11. Agy - 4.11

^a Kg₀ is calculated by means of Voigt–Reuss-Hill approximation. ^b Equation-of-state parameters from data of Thomson et al. (2019), Shim et al. (2000), and Chen et al. (2018). ^c The chemical composition is inferred from the unit-cell volume in ambient conditions. ^d K₇^r is fixed to 4. Cub. Tet, and Orth represent cubic, terragonal, and orthorhombic Ca-Pv. DFT: density functional theory. MD: molecular dynamics. LDA: local density approximation. GGA: generalized gradient approximation. DAC: diamond anvil cell. LVP: large-volume press. XRD: X-ray diffraction. UI: ultrasonic interferometry. BS: Brillouin scattering.

 $d^2 \rho / dX^2$ P (GPa) $d\rho / dX$ dC_{11}/dX dG/dX dC_{12}/dX dC_{44}/dX dK_S / dX dV_P / dX dV_S / dX 20 0.21 -0.31211.1 -69.6-181.1-42.5-85.3-1.27-1.2930 -0.2920.20 -70.9-189.9-41.6-92.616.6 -1.27-1.3380 -0.2400.17 44.2 -89.4-249.4-44.5-135.6-1.43-1.65130 -0.2340.20 63.6 -97.8-304.8-44.2-178.6-1.56-1.91

Table 3. The compositional derivatives of density, elastic constants, elastic moduli, and wave velocities of cubic Ca-Pv at 20, 30, 80, and 100 GPa.

X is the molar fraction of CaTiO₃.

tionships with CaTiO₃ content. The compositional derivatives of density $(d\rho / dX)$ and $d^2\rho / dX^2$, elastic constants (dC_{ij}/dX) , elastic moduli (dK/dX) and dG/dX, and wave velocities $(dV_P / dX \text{ and } dV_S / dX)$ at 20, 30, 80, and 100 GPa are summarized in Table 3, where X denotes the molar fraction of CaTiO₃. The density of Ca-Pv increases with pressure but decreases with increasing CaTiO₃ content (Figs. 3a and 5a). Among the elastic constants, dC_{11}/dX is positive, while dC_{12}/dX and dC_{44}/dX are negative at all four pressures, indicating that C_{11} increases while C_{12} and C_{44} decrease with the addition of CaTiO₃ (Fig. 4). Both K_S and G decrease with increasing CaTiO₃ content. Notably, cubic CaSi_{0.5}Ti_{0.5}O₃ has a lower K_S ($\sim 3.1\%$) and significantly lower G ($\sim 23\%$) than cubic CaSiO₃ at 130 GPa (Fig. 4b). This suggests that the incorporation of Ti into cubic Ca-Pv has a more pronounced effect on shear properties than on compressional properties, primarily due to the strong compositional influence on C_{44} . Consequently, the wave velocities of cubic Ca-Pv decrease with increasing Ti content (Fig. 5b). At 130 GPa, the V_P and V_S of cubic CaSi_{0.5}Ti_{0.5}O₃ are reduced by approximately 5.3 % and 12 %, respectively, compared to those of cubic CaSiO₃.

To understand the evolution of velocity anisotropy in cubic Ca-Pv at high pressures, the anisotropy for V_P (AV_P) and the maximum anisotropy for V_S (AV_S) are defined as follows (Mainprice, 1990):

$$AV_{P} = \frac{V_{P,\text{max}} - V_{P,\text{min}}}{V_{P,\text{max}} + V_{P,\text{min}}} \times 200\%, \tag{15}$$

$$AV_{P} = \frac{V_{P,\text{max}} - V_{P,\text{min}}}{V_{P,\text{max}} + V_{P,\text{min}}} \times 200\%,$$

$$AV_{S} = \left(\frac{V_{S1} - V_{S2}}{V_{S1} + V_{S2}}\right)_{\text{max}} \times 200\%,$$
(15)

where $V_{P,\text{max}}$ and $V_{P,\text{min}}$ represent the maximum and minimum compressional velocities, respectively, and V_{S1} and V_{S2} are two orthogonally polarized shear velocities in a given propagation direction. As shown in Fig. 6, both AV_P and AV_S of cubic CaSiO₃ decrease with pressure and have trends consistent with those of previous theoretical studies (Karki and Crain, 1998; Kawai and Tsuchiya, 2015). Cubic CaSiO₃ has small AV_P and AV_S values at 130 GPa ($AV_P = 0.3\%$ and $AV_S = 0.7 \%$). There is an enhanced composition effect on velocity anisotropies of cubic Ca-Pv at high pressures. The anisotropies of V_P and V_S in $CaSi_{0.875}Ti_{0.125}O_3$ and CaSi_{0.75}Ti_{0.25}O₃ initially decrease with increasing pressure,

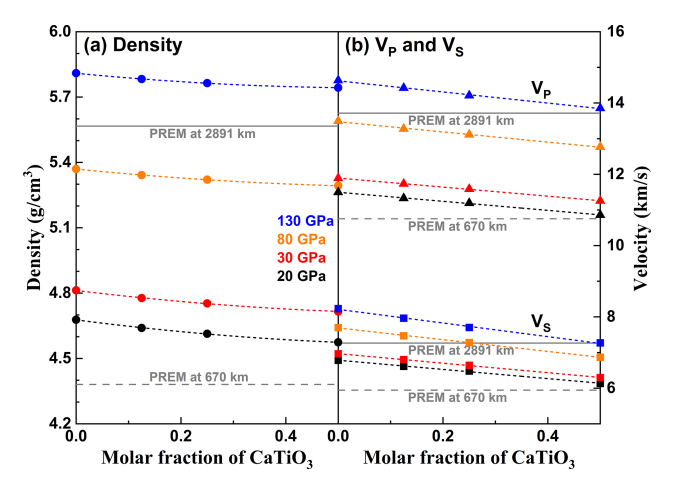


Figure 5. Densities and wave velocities of cubic CaSiO₃-CaTiO₃ perovskites at 20 GPa (black), 30 GPa (red), 80 GPa (orange), and 130 GPa (blue). Symbols and dashed curves are calculated values and fitting results, respectively. Dashed and solid grey lines represent the density and velocities of the preliminary reference Earth model at 670 and 2891 km, respectively.

reaching minimum values at approximately 70 and 30 GPa, respectively, before increasing again at higher pressures. In contrast, AV_P and AV_S values of CaSi_{0.5}Ti_{0.5}O₃ continuously increase with pressure, reaching $\sim 12\%$ and $\sim 30\%$, respectively, at 130 GPa. The elastic anisotropy of cubic crystals can also be quantified using the Zener ratios, defined as A = $2C_{44}/(C_{11}-C_{12})$, where A=1 indicates elastic isotropy. As shown in Fig. S2, the Zener ratio of cubic CaSiO₃ decreases with increasing pressure and approaches unity at \sim 125 GPa. For Ti-bearing Ca-Pv (CaSi_{0.875}Ti_{0.125}O₃, CaSi_{0.75}Ti_{0.25}O₃, and CaSi_{0.5}Ti_{0.5}O₃), the Zener ratios also decrease with pressure, crossing the isotropic value of 1 at approximately 5, 25, and 65 GPa, respectively. The transition from A > 1 to A < 1significantly alters the directional dependence of V_S . Specifically, the fastest V_S , which propagates along the [100] direction when A > 1, shifts to the [111] direction when A < 1. Conversely, the slowest V_S , initially along [111] for A > 1, shifts to the [100] direction for A < 1.

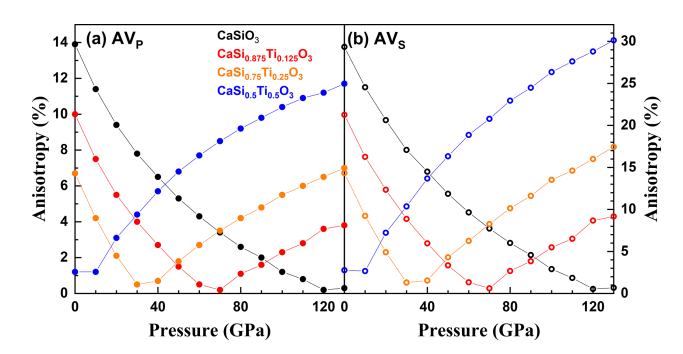


Figure 6. Velocity anisotropies of cubic $CaSiO_3$ – $CaTiO_3$ perovskites at high pressures. Black, red, orange, and blue circles represent $CaSiO_3$, $CaSi_{0.875}Ti_{0.125}O_3$, $CaSi_{0.75}Ti_{0.25}O_3$, and $CaSi_{0.5}Ti_{0.5}O_3$, respectively. Solid and open circles stand for AV_P and AV_S , respectively.

4 Implications

Our results suggest that the acoustic wave velocities of cubic Ca-Pv significantly decrease with increasing Ti content (Fig. 5). Considering the temperature effect predicted by Kawai and Tsuchiya (2015), the cubic Ca-Pv's velocity profiles can be substantially reduced with the addition of Ti in lower-mantle conditions. Thus, it is expected that cubic Tibearing Ca-Pv can reduce the seismic velocity of subducted oceanic crust in the lower mantle because the amount of Ca-Pv in basalt is up to \sim 29 vol. % (Ricolleau et al., 2010). In addition, Ca-Pv in subducted MORB assemblages has a composition of $CaSi_{1-x}Ti_xO_3$ with 0 < x < 0.45 (Litasov and Ohtani, 2005; Hirose and Fei, 2002; Ricolleau et al., 2010). Ca-Pv discovered in "super-deep" diamonds has a detectable content of Ti (Nestola et al., 2018; Walter et al., 2011). However, although our theoretical results in static conditions demonstrate that incorporation of Ti into Ca-Pv significantly reduces its wave velocities at lower-mantle pressures, further experimental or computational studies of the temperature effect on elasticities and velocities of Ti-bearing Ca-Pv are required to determine whether or not its sound velocities explain observed seismic velocity anomalies associated with subducted oceanic crust in Earth's lower mantle (Garnero et al., 2016).

Although Ca-Pv adopts a cubic structure in the lower mantle, it exhibits significant seismic velocity anisotropy in the transition zone and the uppermost lower mantle. Kawai and Tsuchiya (2015) have proposed that cubic CaSiO₃ has the largest anisotropy at the lower part of the mantle transition zone; even a small amount of cubic CaSiO₃ could produce detectable anisotropy. Our calculations confirm this point of view. Thus, seismic anisotropy observed in the mantle transition zone associated with the subducted slabs may be derived from highly anisotropic Ca-Pv (Foley and Long, 2011). More importantly, it is noteworthy that there is an enhanced composition effect on velocity anisotropies of cu-

bic CaSiO₃-CaTiO₃ with Ti content. Incorporation of Ti into Ca-Pv significantly increases its velocity anisotropies, especially for shear velocity, at lower-mantle pressures. Cubic $CaSi_{0.5}Ti_{0.5}O_3$ is highly anisotropic with AV_P and AV_S values of up to $\sim 12\%$ and $\sim 30\%$, respectively, at the lowermost mantle pressure. These values are larger than those of ferropericlase (AV_P: $\sim 10\%$ and AV_S: $\sim 23\%$) and bridgmanite (AV_P : ~ 12 %; AV_S : ~ 16 %) (Yang et al., 2016; Kawai and Tsuchiya, 2015; Kurnosov et al., 2017; Fu et al., 2018) and comparable with those of MgSiO₃ post-perovskite (Mg-PPv) (AV_P : ~15 %; AV_S : ~30 %) (Tsuchiya et al., 2004). The anisotropies of Ti-bearing Ca-Pv in lower-mantle conditions can be much larger than results in static conditions, taking into account the temperature effect based on the results by Kawai and Tsuchiya (2015). Although Mg-PPv is believed to be the major origin of seismic anisotropies in the lowermost mantle and D'' layer (Wu et al., 2017; Garnero and Mcnamara, 2008), our results indicate that Ti-bearing Ca-Pv is highly anisotropic and may be an additional source of seismic anisotropies in the lowermost mantle.

Data availability. All data are presented in the paper (Fig. 2).

Supplement. The supplement related to this article is available online at https://doi.org/10.5194/ejm-37-773-2025-supplement.

Competing interests. The author has declared that there are no competing interests.

Disclaimer. Publisher's note: Copernicus Publications remains neutral with regard to jurisdictional claims made in the text, published maps, institutional affiliations, or any other geographical representation in this paper. While Copernicus Publications makes every effort to include appropriate place names, the final responsibility lies with the authors. Views expressed in the text are those of the authors and do not necessarily reflect the views of the publisher.

Acknowledgements. I acknowledge Bingtian Tu for providing computational resources and Shengxuan Huang for constructive suggestions.

Financial support. This research has been supported by the National Natural Science Foundation of China (grant nos. 42274123 and 42411540023) and the United Laboratory of High-Pressure Physics and Earthquake Science.

Review statement. This paper was edited by Sandro Jahn and reviewed by two anonymous referees.

References

- Birch, F.: Finite strain isotherm and velocities for single-crystal and polycrystalline NaCl at high pressures and 300 K, J. Geophys. Res.-Sol. Ea., 83, 1257–1268, https://doi.org/10.1029/JB083iB03p01257, 1978.
- Blöchl, P. E.: Projector augmented-wave method, Phys. Rev. B, 50, 17953–17979, https://doi.org/10.1103/PhysRevB.50.17953, 1994.
- Ceperley, D. M. and Alder, B. J.: Ground state of the electron gas by a stochastic method, Phys. Rev. Lett., 45, 566–569, https://doi.org/10.1103/PhysRevLett.45.566, 1980.
- Chao, K.-H., Berrada, M., Wang, S., Peckenpaugh, J., Zhang, D., Chariton, S., Prakapenka, V., and Chen, B.: Structure and equation of state of Ti-bearing davemaoite: New insights into the chemical heterogeneity in the lower mantle, Am. Mineral., 109, 1861–1870, https://doi.org/10.2138/am-2023-9104, 2024.
- Chen, H., Shim, S.-H., Leinenweber, K., Prakapenka, V., Meng, Y., and Prescher, C.: Crystal structure of CaSiO₃ perovskite at 28–62 GPa and 300 K under quasi-hydrostatic stress conditions, Am. Mineral., 103, 462–468, https://doi.org/10.2138/am-2018-6087, 2018.
- Davies, G. F.: Effective elastic moduli under hydrostatic stress-I. quasi-harmonic theory, J. Phys. Chem. Solids, 35, 1513–1520, 1974.
- Essene, E.: High-pressure transformations in CaSiO₃, Contrib. Mineral. Petrol., 45, 247–250, 1974.
- Foley, B. J. and Long, M. D.: Upper and mid-mantle anisotropy beneath the Tonga slab, Geophys. Res. Lett., 38, L02303, https://doi.org/10.1029/2010GL046021, 2011.
- Fu, S., Yang, J., Zhang, Y., Okuchi, T., Mccammon, C., Kim, H. I., Lee, S. K., and Lin, J. F.: Abnormal Elasticity of Fe-Bearing Bridgmanite in the Earth's Lower Mantle, Geophys. Res. Lett., 45, 4725–4732, https://doi.org/10.1029/2018GL077764, 2018.
- Garnero, E. J. and Mcnamara, A. K.: Structure and Dynamics of Earth's Lower Mantle, Science, 320, 626–628, https://doi.org/10.1126/science.1148028, 2008.
- Garnero, E. J., Mcnamara, A. K., and Shim, S. H.: Continent-sized anomalous zones with low seismic velocity at the base of Earth's mantle, Nat. Geosci., 9, 481–489, https://doi.org/10.1038/ngeo2733, 2016.
- Gasparik, Tibor, Wolf, and Kenneth: Experimental determination of phase relations in the CaSiO₃ system from 8 to 15 GPa, Am. Mineral., 79, 1219–1222, 1994.
- Gréaux, S., Irifune, T., Higo, Y., Tange, Y., Arimoto, T., Liu, Z., and Yamada, A.: Sound velocity of CaSiO₃ perovskite suggests the presence of basaltic crust in the Earth's lower mantle, Nature, 565, 218–222, https://doi.org/10.1038/s41586-018-0816-5, 2019.
- Guennou, M., Bouvier, P., Krikler, B., Kreisel, J., Haumont, R., and Garbarino, G.: High-pressure investigation of CaTiO₃ up to 60 GPa using X-ray diffraction and Raman spectroscopy, Phys. Rev. B, 82, 134101, https://doi.org/10.1103/PhysRevB.82.134101, 2010.
- Hill, R.: The elastic behaviour of a crystalline aggregate, Proc. Phys. Soc. A, 65, 349, https://doi.org/10.1088/0370-1298/65/5/307, 1952.

- Hirose, K.: Phase transitions in pyrolitic mantle around 670-km depth: Implications for upwelling of plumes from the lower mantle, J. Geophys. Res.-Sol. Ea., 107, ECV 3-1–ECV 3-13, 2002.
- Hirose, K. and Fei, Y.: Subsolidus and melting phase relations of basaltic composition in the uppermostlower mantle, Geochim. Cosmochim. Ac., 66, 2099–2108, https://doi.org/10.1016/S0016-7037(02)00847-5, 2002.
- Irifune, T., Shinmei, T., McCammon, C. A., Miyajima, N., Rubie, D. C., and Frost, D. J.: Iron partitioning and density changes of pyrolite in Earth's lower mantle, Science, 327, 193–195, https://doi.org/10.1126/science.1181443, 2010.
- Karki, B. B. and Crain, J.: First-principles determination of elastic properties of CaSiO₃ perovskite at lower mantle pressures, Geophys. Res. Lett., 25, 2741–2744, https://doi.org/10.1029/98GL51952, 1998.
- Kawai, K. and Tsuchiya, T.: Small shear modulus of cubic CaSiO₃ perovskite, Geophys. Res. Lett., 42, 2718–2726, https://doi.org/10.1002/2015GL063446, 2015.
- Kesson, S., Fitz Gerald, J., and Shelley, J.: Mineralogy and dynamics of a pyrolite lower mantle, Nature, 393, 252–255, 1998.
- Komabayashi, T., Hirose, K., Sata, N., Ohishi, Y., and Dubrovinsky, L. S.: Phase transition in CaSiO₃ perovskite, Earth Planet. Sc. Lett., 260, 564–569, https://doi.org/10.1016/j.epsl.2007.06.015, 2007.
- Kresse, G. and Furthmüller, J.: Efficient iterative schemes for ab initio total-energy calculations using a plane-wave basis set, Phys. Rev. B, 54, 11169, https://doi.org/10.1103/PhysRevB.54.11169, 1996
- Kresse, G. and Joubert, D.: From ultrasoft pseudopotentials to the projector augmented-wave method, Phys. Rev. B, 59, 1758, https://doi.org/10.1103/PhysRevB.59.1758, 1999.
- Kubo, A., Suzuki, T., and Akaogi, M.: High pressure phase equilibria in the system CaTiO₃-CaSiO₃: stability of perovskite solid solutions, Phys. Chem. Miner., 24, 488–494, https://doi.org/10.1007/s002690050063, 1997.
- Kudo, Y., Hirose, K., Murakami, M., Asahara, Y., Ozawa, H., Ohishi, Y., and Hirao, N.: Sound velocity measurements of CaSiO₃ perovskite to 133 GPa and implications for lowermost mantle seismic anomalies, Earth Planet. Sc. Lett., 349, 1–7, https://doi.org/10.1016/j.epsl.2012.06.040, 2012.
- Kurnosov, A., Marquardt, H., Frost, D. J., Ballaran, T. B., and Ziberna, L.: Evidence for a Fe³⁺-rich pyrolitic lower mantle from (Al,Fe)-bearing bridgmanite elasticity data, Nature, 543, 543–546, https://doi.org/10.1038/nature21390, 2017.
- Li, B., Kung, J., and Liebermann, R. C.: Modern techniques in measuring elasticity of Earth materials at high pressure and high temperature using ultrasonic interferometry in conjunction with synchrotron X-radiation in multi-anvil apparatus, Phys. Earth Planet. Inter., 143, 559–574, https://doi.org/10.1016/j.pepi.2003.09.020, 2004.
- Li, L., Weidner, D. J., Brodholt, J., Alfe, D., David Price, G., Caracas, R., and Wentzcovitch, R.: Elasticity of CaSiO₃ perovskite at high pressure and high temperature, Phys. Earth Planet. Inter., 155, 249–259, https://doi.org/10.1016/j.pepi.2005.12.006, 2006.
- Litasov, K. D. and Ohtani, E.: Phase relations in hydrous MORB at 18–28 GPa: implications for heterogeneity of the lower mantle, Phys. Earth Planet. Inter., 150, 239–263, https://doi.org/10.1016/j.pepi.2004.10.010, 2005.

- Mainprice, D.: A FORTRAN program to calculate seismic anisotropy from the lattice preferred orientation of minerals, Comput. Geosci., 16, 385–393, https://doi.org/10.1016/0098-3004(90)90072-2, 1990.
- Mao, H. K., Chen, L. C., Hemley, R. J., Jephcoat, A. P., Wu, Y., and Bassett, W. A.: Stability and equation of state of CaSiO₃-Perovskite to 134 GPa, J. Geophys. Res.-Atmos., 94, 17889–17894, https://doi.org/10.1029/JB094iB12p17889, 1989.
- Monkhorst, H. J. and Pack, J. D.: Special points for Brillouin-zone integrations, Phys. Rev. B, 13, 5188, https://doi.org/10.1103/PhysRevB.13.5188, 1976.
- Murakami, M., Ohishi, Y., Hirao, N., and Hirose, K.: A perovskitic lower mantle inferred from high-pressure, high-temperature sound velocity data, Nature, 485, 90–94, https://doi.org/10.1038/nature11004, 2012.
- Nestola, F., Korolev, N., Kopylova, M., Rotiroti, N., Pearson, D. G., Pamato, M. G., Alvaro, M., Peruzzo, L., Gurney, J. J., and Moore, A. E.: CaSiO₃ perovskite in diamond indicates the recycling of oceanic crust into the lower mantle, Nature, 555, 237–241, https://doi.org/10.1038/nature25972, 2018.
- Noguchi, M., Komabayashi, T., Hirose, K., and Ohishi, Y.: High-temperature compression experiments of CaSiO₃ perovskite to lowermost mantle conditions and its thermal equation of state, Phys. Chem. Miner., 40, 81–91, https://doi.org/10.1007/s00269-012-0549-1, 2013.
- Ono, S., Ito, E., and Katsura, T.: Mineralogy of subducted basaltic crust (MORB) from 25 to 37 GPa, and chemical heterogeneity of the lower mantle, Earth Planet. Sci. Lett., 190, 57–63, 2001.
- Ono, S., Ohishi, Y., and Mibe, K.: Phase transition of Ca-perovskite and stability of Al-bearing Mg-perovskite in the lower mantle, Am. Mineral., 89, 1480–1485, https://doi.org/10.2138/am-2004-1016, 2004.
- Perdew, J. P. and Zunger, A.: Self-interaction correction to densityfunctional approximations for many-electron systems, Phys. Rev. B, 23, 5048–5079, https://doi.org/10.1103/PhysRevB.23.5048, 1981.
- Ricolleau, A., Perrillat, J. P., Fiquet, G., Daniel, I., Matas, J., Addad, A., Menguy, N., Cardon, H., Mezouar, M., and Guignot, N.: Phase relations and equation of state of a natural MORB: Implications for the density profile of subducted oceanic crust in the Earth's lower mantle, J. Geophys. Res., 115, B08202, https://doi.org/10.1029/2009JB006709, 2010.
- Sagatova, D., Shatskiy, A., Sagatov, N., and Litasov, K.: Phase relations in CaSiO₃ system up to 100 GPa and 2500 K, Geochemistry International, 59, 791–800, https://doi.org/10.1134/S0016702921080073, 2021.
- Shim, S. H., Duffy, T. S., and Shen, G.: The stability and P-V-T equation of state of CaSiO₃ perovskite in the Earth's lower mantle, J. Geophys. Res.-Sol. Ea., 105, 25955–25968, https://doi.org/10.1029/2000JB900183, 2000.
- Shim, S. H., Jeanloz, R., and Duffy, T. S.: Tetragonal structure of CaSiO₃ perovskite above 20 GPa, Geophys. Res. Lett., 29, 19-11–19-14, https://doi.org/10.1029/2002GL016148, 2002.
- Sinelnikov, Y. D., Chen, G., and Liebermann, R. C.: Elasticity of CaTiO₃-CaSiO₃ perovskites, Phys. Chem. Miner., 25, 515–521, https://doi.org/10.1007/s002690050143, 1998.

- Stixrude, L., Lithgow-Bertelloni, C., Kiefer, B., and Fumagalli, P.: Phase stability and shear softening in CaSiO₃ perovskite at high pressure, Phys. Rev. B, 75, 024108, https://doi.org/10.1103/PhysRevB.75.024108, 2007.
- Sueda, Y., Irifune, T., Yamada, A., Inoue, T., Liu, X., and Funakoshi, K. I.: The phase boundary between $CaSiO_3$ perovskite and $Ca_2SiO_4 + CaSi_2O_5$ determined by in situ X-ray observations, Geophys. Res. Lett., 33, L10307, https://doi.org/10.1029/2006GL025772, 2006.
- Sun, N., Mao, Z., Yan, S., Wu, X., Prakapenka, V., and Lin, J.-F.: Confirming a pyrolitic lower mantle using self-consistent pressure scales and new constraints on CaSiO₃ perovskite, J. Geophys. Res.-Sol. Ea., 121, 4876–4894, https://doi.org/10.1002/2016JB013062, 2016.
- Sun, N., Bian, H., Zhang, Y., Lin, J.-F., Prakapenka, V. B., and Mao, Z.: High-pressure experimental study of tetragonal CaSiO₃-perovskite to 200 GPa, Am. Mineral., 107, 110–115, https://doi.org/10.2138/am-2021-7913, 2022.
- Thomson, A. R., Crichton, W. A., Brodholt, J. P., Wood, I. G., Siersch, N. C., Muir, J. M. R., Dobson, D. P., and Hunt, S. A.: Seismic velocities of CaSiO₃ perovskite can explain LLSVPs in Earth's lower mantle, Nature, 572, 643–647, https://doi.org/10.1038/s41586-019-1483-x, 2019.
- Truffet, B., Fiquet, G., Morard, G., Baron, M., Miozzi, F., Harmand, M., Ravasio, A., Mezouar, M., and Guyot, F.: High pressure dissociation of CaTiO₃ perovskite into CaO and CaTi₂O₅, Phys. Earth Planet. Inter., 334, 106968, https://doi.org/10.1016/j.pepi.2022.106968, 2023.
- Tschauner, O., Huang, S., Yang, S., Humayun, M., Liu, W., Gilbert Corder, S. N., Bechtel, H. A., Tischler, J., and Rossman, G. R.: Discovery of davemaoite, CaSiO₃-perovskite, as a mineral from the lower mantle, Science, 374, 891–894, https://doi.org/10.1126/science.abl8568, 2021.
- Tsuchiya, T., Tsuchiya, J., Umemoto, K., and Wentzcovitch, R. M.: Elasticity of post-perovskite MgSiO₃, Geophys. Res. Lett., 31, L14603, https://doi.org/10.1029/2004GL020278, 2004.
- Walter, M. J., Kohn, S. C., Araujo, D., Bulanova, G. P., Smith, C. B., Gaillou, E., Wang, J., Steele, A., and Shirey, S. B.: Deep mantle cycling of oceanic crust: evidence from diamonds and their mineral inclusions, Science, 334, 54–57, https://doi.org/10.1126/science.1209300, 2011.
- Wang, Y., Weidner, D. J., and Guyot, F.: Thermal equation of state of CaSiO₃ perovskite, J. Geophys. Res.-Sol. Ea., 101, 661–672, https://doi.org/10.1029/95JB03254, 1996.
- Wu, X., Lin, J. F., Kaercher, P., Mao, Z., Liu, J., Wenk, H. R., and Prakapenka, V. B.: Seismic anisotropy of the *D*" layer induced by (001) deformation of post-perovskite, Nat. Commun., 8, 14669, https://doi.org/10.1038/ncomms14669, 2017.
- Yang, J., Lin, J. F., Jacobsen, S. D., Seymour, N. M., and Prakapenka, V. B.: Elasticity of Ferropericlase and Seismic Heterogeneity in the Earth's Lower Mantle: ferropericlase high P-T elasticity, J. Geophys. Res.-Sol. Ea., 121, 8488–8500, https://doi.org/10.1002/2016JB013352, 2016.
- Yin, K., Belonoshko, A. B., Li, Y., and Lu, X.: Davemaoite as the mantle mineral with the highest melting temperature, Sci. Adv., 9, eadj2660, https://doi.org/10.1126/sciadv.adj2660, 2023.